Modeling Gaussian Beam Propagation in Micro-Droplets with Ray Optics

Rouven H. Klenk[1], Simon Abdani[1], Wolfgang Vogel[1], Manfred Berroth[1], Michael Heymann[2], and Georg Rademacher[1]
[1]*Institute of Electrical and Optical Communications,* [2]*Institute of Biomaterials and Biomolecular Systems*
University of Stuttgart
Stuttgart, Germany
rouven.klenk@int.uni-stuttgart.de

***Abstract*—Grating couplers serve as efficient fiber-chip interfaces. They can also be used to interface optical signals with analytes in optofluidic systems. This study investigates the intensity of a Gaussian beam, emitted from a grating coupler, when interfaced with a droplet. The results can be used to optimize the geometrical setup to maximize the interaction of the optical signal with the analyte. The presented approach can be used as a tool to simplify numerical implementations of droplets in optical simulations.**

Keywords—photonics, optofluidics, droplets, ray optics

I. Optofluidic Droplet Assays

Droplet sorters are valuable components of optofluidic assemblies in bio-medical research and biological testing. In such systems, analytes are encapsulated in droplets, guided through microfluidic channels. Previously, fiber-based droplet sorters have been demonstrated, where, i.e. fluorescent analytes are stimulated by light emitted from the tip of an optical fiber [1]. To integrate such optofluidic systems, soft lithography using polydimethylsiloxan (PDMS) is employed. To further enhance the integration density of the optical setup, photonic integrated circuits (PICs) can be combined with PDMS-based microfluidic systems. In this work, a photonic-integrated setup is analyzed, where light for excitation and detection is guided to the microfluidic channel via grating couplers, directed to the passing droplets. Grating couplers use diffraction to vertically couple light in and out of a PIC. To optimize the Bragg grating of the coupler, the optical fiber field is often approximated by a Gaussian beam. Although the diffraction grating limits the bandwidth, proposed solutions mitigate this [2], and the concern primarily applies to multi-color assays. The analysis of particles [3] and fluids [4] has already been demonstrated, with a microfluidic channel above the grating coupler. To ensure complete excitation of the analyte within the droplet, the incoming field must be optimized to illuminate the entire droplet volume uniformly. Therefore, the field inside the droplet has to be modeled. Numerically simulating the grating coupler and droplet within a common finite element framework is resource-intensive due to their size mismatch. Droplets typically range from 50 µm to 100 µm in diameter, while grating couplers have much smaller footprints, around (15 µm)^2. Simulating the curvature of a droplet with sufficient resolution for visible wavelengths requires significant computational resources.

In this work, a Gaussian beam is imaged inside the droplet to describe the field within the droplet. Maximizing the intensity or 3-dB distribution coefficient results in an optimal mode field diameter (MFD) and distance for which the grating coupler can be optimized numerically.

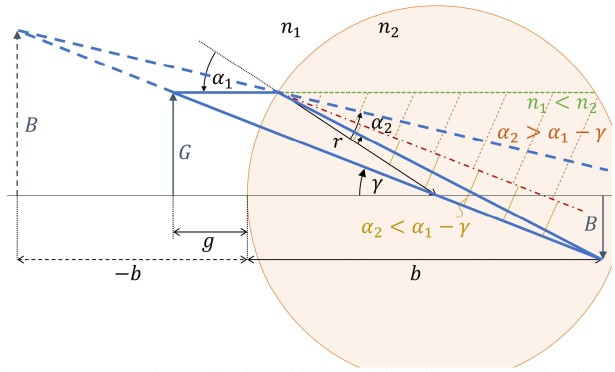

Fig. 1. Ray optics projecting object G with a distance g to the droplet surface resulting in image B with a distance b. Depicted are the ray through the middle of the droplet, and the refracted parallel ray, dependent on the object and the refractive indices.

II. Gauss Image Through Droplet Surface

A droplet is modeled as a perfectly round sphere with refractive index n_2, and radius r as shown in Fig. 1. The surrounding area has a refractive index of n_1. An object with a height G is in front of the droplet with a distance g. To construct the image with the height B, two rays are needed. First, the chief ray, which has an angle of incidence of 0°, passes through the middle of the droplet, due to the perfect spherical shape. Secondly, we consider the ray parallel to the optical axis. Here, the angle of incidence is α_1. Following Snell's law

$$n_1 \sin(\alpha_1) = n_2 \sin(\alpha_2), \tag{1}$$

the transmitted focal ray is refracted and enters the droplet with an angle α_2. The crossing point of these two rays is the image of the point of origin. Repeating this imaging process with every point of the object along G results in the image B. In order to have a high confinement inside the droplet, we assume $n_1 < n_2$ [5]. That limits our imaging to two cases, in which the rays could intersect. One, where the image is inside or behind the droplet

$$\alpha_2 < \alpha_1 - \gamma, \tag{2}$$

and the other with the image in front of the droplet,

$$\alpha_2 > \alpha_1 - \gamma. \tag{3}$$

In case of $\alpha_2 = \alpha_1 - \gamma$, chief ray and focal ray do not intersect, the red dashed-dotted line in Fig. 1.

Given the size ratios considered in this study, the small-angle approximation commonly used in the literature is not applied [6]. As illustrated in Fig. 2, the Gaussian beam within the droplet is a projection of the beam that enters it. Analog to the imaging above, the projected object G corresponds to the waist w_0 of the Gaussian beam and the image B to the waist

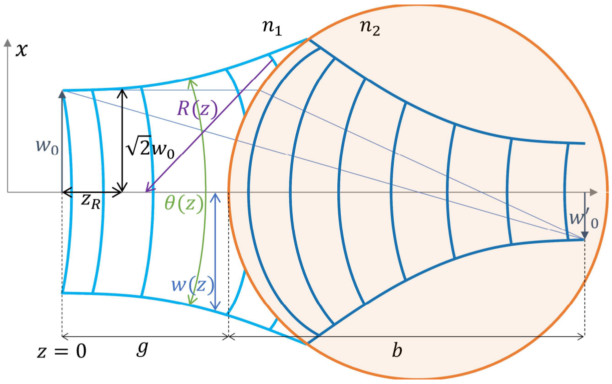

Fig. 2. A gaussian beam originating in $z = 0$ with a waist w_0 and its droplet image originating in $z = g + b$ with an image waist of w'_0. Additionally, the metrices of a Gaussian beam are sketched in the first beam.

w'_0 of the resulting beam inside the droplet. Together with refractive index n_1 and wavelength λ, the waist defines the Gaussian beam

$$E(x,z) = E_0 \frac{w_0}{w(z)} e^{-\left(\frac{x}{w(z)}\right)^2} e^{-i\left(n_1 k_0 z - \theta(z) + \frac{n_1 k_0 x^2}{2R(z)}\right)}, \quad (4)$$

where $w(z)$ is the radius at which the field amplitudes decrease to $1/e$ of their axial values at the plane z along the beam. Perpendicular to the beam is the x-axis. The Gouy phase $\theta(z)$ and the radius of curvature $R(z)$ of the beam's wavefront at position z, together with the wave number k_0, determine the phase of a Gaussian beam. All functions are dependent on the Rayleigh length

$$z_R = \frac{\pi n_1 w_0^2}{\lambda} \quad (5)$$

where the area of the cross section is doubled. The field inside is then dependent on w'_0 and n_2, with the origin at $z = g + b$.

$$E(x,z) \to E'(x, z - g - b); r > \sqrt{x^2 + (z - g - b)^2} \quad (6)$$

The amplitude at the origin

$$E'_0 = E_0 \frac{n_1}{n_2} \sqrt{\frac{1 + \left(\frac{b}{z'_R}\right)^2}{1 + \left(\frac{g}{z_R}\right)^2}} \quad (7)$$

is normalized to keep the intensity constant at perpendicular entrance into the droplet, i.e. $E(0, g) = E'(0, -b)$. Reflections at the surface are negligible for typical values of $n_1 = 1.29$ and $n_2 = 1.54$ [5].

III. Intensity Inside Micro-Droplets

Analyzing droplets optically involves exciting the analyte inside. Hence, the intensity of the excitation light within the droplet

$$I = \frac{\Sigma \frac{|E'|^2}{2} n_2 e^{-z\alpha_{\mathrm{abs}}}}{\pi r^2}, r > \sqrt{x^2 + (z - g - b)^2} \quad (8)$$

is a crucial parameter. Included here is the absorption α_{abs} and the refractive index n_2. In Fig. 3 a) the normalized intensity inside a droplet is calculated over the MFD and the distance g to the droplet surface. The MFD is here the projected object and is double the size of the waist w'_0. The considered droplet has a radius $r = 25$ µm, the refractive indices are set as stated before, and the excitation wavelength is $\lambda = 488$ nm. For a worst-case setting, the absorption is set

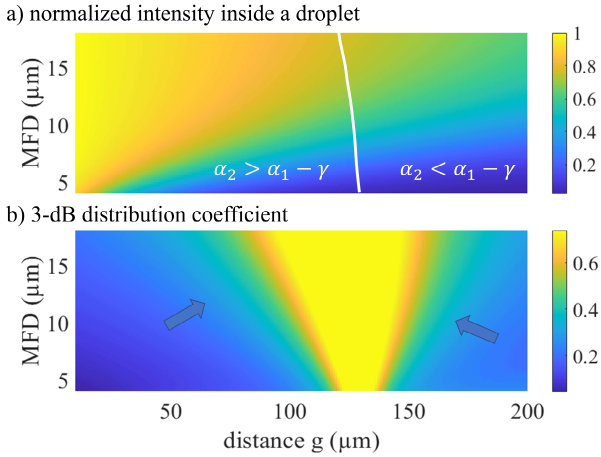

Fig. 3. a) Normalized intensity inside a droplet with $r = 25$ µm, $n_1 = 1.29$, and $n_2 = 1.54$, and b) the 3-dB distribution coefficient.

to the value of PDMS, $\alpha_{\mathrm{abs}} = 20\ \mathrm{cm}^{-1}$ [7]. Depending on the analyte inside the droplet, not only a high intensity, but the intensity distribution within the volume is important. Otherwise, some regions of the droplet may not be excited at all. As a figure of merit, the 3-dB distribution coefficient is defined. For a 2-dimensional case, it is the area inside the droplet where the intensity is greater than 50% of the maximum intensity inside, divided by the total droplet area. The results for varying MFD and distance g are plotted in Fig. 3 b). The measures show different trends. Small distances and large MFDs achieve a high intensity. Meanwhile, the 3-dB distribution coefficient tends towards an optimal configuration, where the distance is between 100 µm and 150 µm. At the same time, the MFD should be as large as possible. The highest 3-dB distribution coefficients are observed along the line defined by $\alpha_2 = \alpha_1 - \gamma$. In theory, the chief and focal rays would intersect at infinity, indicating that ray optics is approaching its limits in this scenario. As a result, interpretations near this region should be approached with caution. Due to the simplifications involved in modeling the Gaussian beam alongside ray optics, the proposed method is intended primarily to identify general trends for optimization. Nonetheless, this model offers a practical and resource-efficient tool for rapid evaluation and optimization tasks.

References

[1] R. H. Cole, N. de Lange, Z. J. Gartner, and A. R. Abate, 'Compact and modular multicolour fluorescence detector for droplet microfluidics', *Lab Chip*, vol. 15, no. 13, Art. no. 13, 2015, doi: 10.1039/C5LC00333D.

[2] R. H. Klenk *et al.*, 'Integrated dispersive structures for bandwidth-enhancement of silicon grating couplers', *Opt Quant Electron*, vol. 52, no. 2, Art. no. 2, Feb. 2020, doi: 10.1007/s11082-020-2194-0.

[3] S. Kerman *et al.*, 'Integrated Nanophotonic Excitation and Detection of Fluorescent Microparticles', *ACS Photonics*, vol. 4, no. 8, Art. no. 8, Aug. 2017, doi: 10.1021/acsphotonics.7b00171.

[4] R. H. Klenk *et al.*, 'Grating Couplers for Chip-Integrated Optofluidic Fluorescence Quantification', in *2021 Kleinheubach Conference*, Miltenberg, Germany: IEEE, Sep. 2021, pp. 1–3. doi: 10.23919/IEEECONF54431.2021.9598417.

[5] S. K. Y. Tang *et al.*, 'A multi-color fast-switching microfluidic droplet dye laser', *Lab Chip*, vol. 9, no. 19, Art. no. 19, 2009, doi: 10.1039/b914066b.

[6] E. Hecht, *Optics*, 5 edition. Global edition. Boston: Pearson Education, Inc, 2017.

[7] S. Alfihed, M. H. Bergen, J. F. Holzman, and I. G. Foulds, 'A detailed investigation on the terahertz absorption characteristics of polydimethylsiloxane (PDMS)', *Polymer*, vol. 153, pp. 325–330, Sep. 2018, doi: 10.1016/j.polymer.2018.08.025.